iScience

Article

Modeling autoregulation of cardiac excitation-Ca-contraction and arrhythmogenic activities in response to mechanical load changes

Graphical abstract

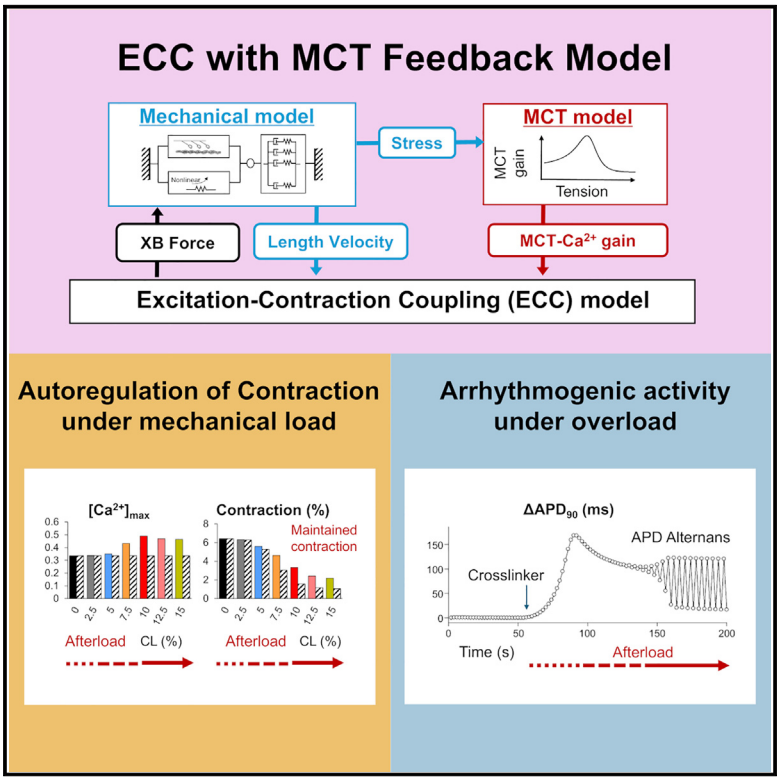

Highlights

- Mechano-chemo-transduction (MCT) mechanism adjusts MCT-Ca^{2+} gain in cardiomyocytes
- Our new model integrates the MCT feedback into excitation-Ca^{2+}-contraction model
- The model reproduces autoregulation of contractility in response to load changes
- The model can also reproduce arrhythmogenic alternans under overload conditions

Authors

Asuka Hatano, Leighton T. Izu, Ye Chen-Izu, Daisuke Sato

Correspondence

hatano@fml.t.u-tokyo.ac.jp (A.H.), ltizu@ucdavis.edu (L.T.I.)

In brief

Cardiovascular medicine; Cell biology; Bioinformatics

Hatano et al., 2025, iScience *28*, 111788
February 21, 2025
https://doi.org/10.1016/j.isci.2025.111788

CellPress

iScience

CellPress
OPEN ACCESS

Article

Modeling autoregulation of cardiac excitation-Ca-contraction and arrhythmogenic activities in response to mechanical load changes

Asuka Hatano,[1,2,5,*] Leighton T. Izu,[1,*] Ye Chen-Izu,[1,3,4] and Daisuke Sato[1]
[1]Department of Pharmacology, University of California – Davis, Davis, CA 94040, USA
[2]Department of Mechanical Engineering, University of Tokyo, Tokyo 113-8656, Japan
[3]Department of Biomedical Engineering, University of California – Davis, Davis, CA 94040, USA
[4]Department of Internal Medicine/Cardiology, University of California – Davis, Davis, CA 94040, USA
[5]Lead contact
*Correspondence: hatano@fml.t.u-tokyo.ac.jp (A.H.), ltizu@ucdavis.edu (L.T.I.)
https://doi.org/10.1016/j.isci.2025.111788

SUMMARY

The heart has intrinsic abilities to autoregulate contractile force in response to mechanical load. Recent experimental studies show that cardiomyocytes have mechano-chemo-transduction (MCT) mechanisms that form a closed feedback loop in the excitation-Ca^{2+} signaling-contraction (E-C) coupling. This closed feedback loop enables autoregulation of contraction in response to mechanical load changes. Here, we develop the first autoregulatory E-C coupling model that couples electrophysiology, Ca^{2+} signaling, force development and contraction, and MCT feedback. The model recapitulates the experimental data showing that the mechanical load on cardiomyocytes during contraction increases the L-type Ca^{2+} current, action potential duration, sarcoplasmic reticulum (SR) Ca^{2+} content, and SR Ca^{2+} release, giving rise to increased cytosolic Ca^{2+} transient (MCT-Ca^{2+} gain) and enhanced contraction. The model also makes non-trivial predictions on the autoregulation of contraction with moderate MCT-Ca^{2+} gain under a range of physiological load changes, but arrhythmogenic discordant alternans with excessive MCT-Ca^{2+} gain under pathological overload.

INTRODUCTION

The heart autoregulate its contraction force in response to both preload[1,2] and afterload.[2–4] This intrinsic ability to adjust contractile force is an important mechanism to maintain cardiac output under changing hemodynamic conditions. There is consensus that many ion channels are mechanically modulated,[5–7] and these mechano-sensitive channels affect cardiac electrophysiology.[8–10] For example, action potential alteration upon externally induced stretch has been explained by currents through stretch-activated channels. Calcium (Ca^{2+}) handling alteration including increased RyR open probability and change in affinity of troponin C for Ca^{2+} also affect electrophysiology via triggered Ca^{2+}-waves and accompanying depolarization.[11] In existing models the amplitudes and kinetics of their mechanical modulation, as well as the molecular mechanisms, are still to be elucidated.[12,13]

The cell-in-gel technique was developed to impose a mechanical load on a contracting cardiomyocyte to simulate increased afterload in the working heart.[14,15] In the cell-in-gel approach, isolated cardiomyocytes are embedded in a 3-dimensional (3D) viscoelastic hydrogel polymer matrix, which more closely mimics the physiological 3D mechanical environment compared to the previous studies using 1D uniaxial stretch.[16–19] Cell-in-gel studies have shown that intracellular Ca^{2+} transient and diastolic Ca^{2+} sparks increased in the cardiomyocytes contracting in-gel under mechanical load. Mechano-chemo-transduction (MCT), processes that convert mechanical signals to intracellular signals, that underlie changes in Ca^{2+} dynamics in cell-in-gel experiments is dependent on localized nitric oxide synthase 1 (NOS1) and Ca^{2+}/calmodulin-dependent protein kinase II (CaMKII) signaling.[15] To elucidate the ionic mechanisms underlying mechano-electric coupling (MEC), we further performed patch-clamp-in-gel[20] experiments using rabbit ventricular myocyte and found that the afterload on a contracting cardiomyocyte regulates multiple ionic currents including L-type Ca^{2+} current ($I_{Ca,L}$), transient outward K current (I_{to}), inward rectifier K current (I_{K1}), leading to prolonged action potential duration (APD) and enhanced Ca^{2+} transient (called MCT-Ca^{2+} gain). The MCT-Ca^{2+} gain increases with increasing load, which maintains the contraction amplitude in a range of varying loads, demonstrating cardiomyocytes' ability to auto-regulate their contraction.[21]

Importantly, excessively high loads promoted the development of electromechanical discordant alternans in APD and contraction amplitudes. Electromechanical discordant alternans is characterized by long action potentials corresponding to small Ca^{2+} transients and contractions,[22,23] in contrast to the electromechanical concordant alternans where long action potentials correspond to large Ca^{2+} transients. Interestingly, the cardiomyocytes

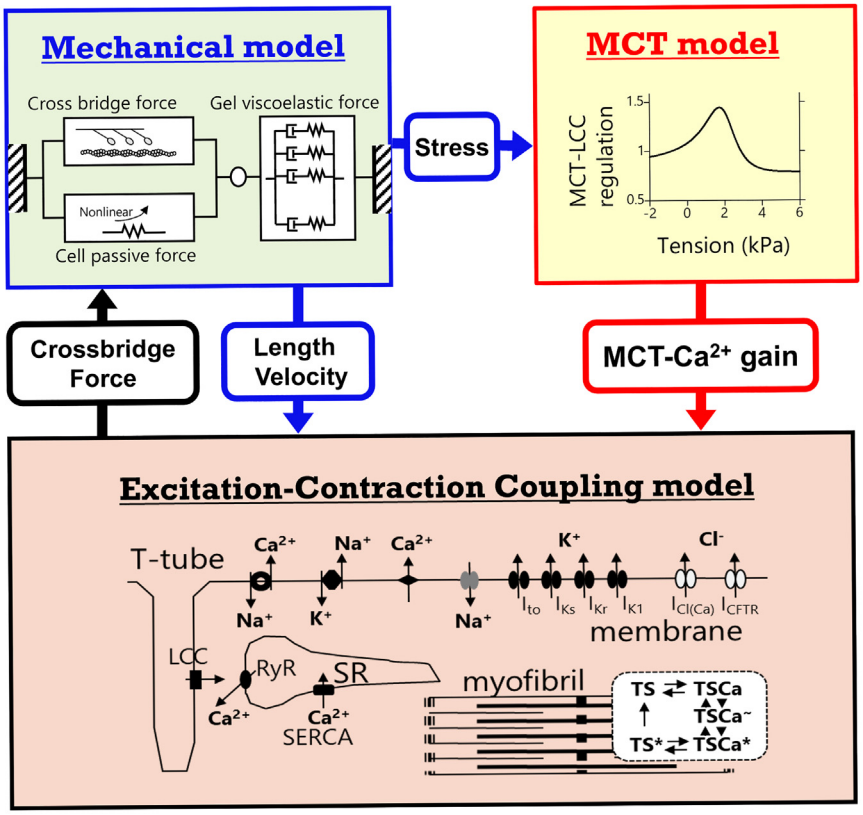

Figure 1. EC coupling with MCT feedback model

The electrophysiology model by Shannon et al.[28] and cross-bridge force development model by Negroni et al.[29] shown at the bottom were implemented, referring to length and velocity calculated in the mechanical model and MCT-Ca^{2+} gain for LCC upregulation. The mechanical model shown in the blue box is simplified to 1° of freedom, to calculate the equilibrium between cross-bridge force from the EC coupling model, nonlinear cell-passive force, and gel-viscoelastic force expressed by the generalized Maxwell model. Calculated stress feedback to EC coupling model through Mechano-chemo-transduction (MCT) model shown in red. The MCT-Ca^{2+} gain function relates the cell-edge tension loaded by the gel to the L-type Ca^{2+} Chennel upregulation coefficient. This MCT feedback autoregulates contraction in our proposed system.

under load-free conditions typically exhibit electromechanical concordant alternans, whereas the cardiomyocytes under mechanical load in the cell-in-gel experiment consistently exhibited electromechanical discordant alternans. This divergent behavior needs to be addressed by modeling the E-C coupling dynamics system in the cardiomyocytes under mechanical load.

Contraction autoregulation was first predicted by Izu et al.[21] that was confirmed experimentally.[24] This model provided the broad outline of the cellular mechanisms sufficient to produce constant contraction amplitude despite changes in mechanical load. Kazemi-Lari et al. then developed a phenomenological model of the autoregulation of contractility in cardiomyocytes using a viscoelastic Eshelby model.[25,26] The responses of this model were studied analytically assuming an ellipsoidal cell and numerically with finite element model based on morphological measurements of cardiomyocytes. The model quantitatively reproduced MCT-Ca^{2+} gain and estimated the 3D stress history of the cell and the gel. However, in this model, the cell strain modulates intracellular Ca^{2+} concentration ($[Ca^{2+}]$) values but without electrophysiological details, such as action potential, ion currents, or intra sarcoplasmic reticulum (SR) calcium, $[Ca^{2+}]_{SR}$. Electrophysiology is a complex dynamical system[22,27]; and well-tuned models are already established.[28–32]

To investigate the effects of mechanical feedback on the chemical and electrical dynamics of a cardiomyocyte, we developed an MCT model by coupling electrophysiology, Ca^{2+} signaling, cross-bridge-force development, and mechanical contraction (Figure 1). The mechanical model used here is a model solving equilibrium between a viscoelastic gel element and a hyperelastic cell element with an input of cross-bridge force. In this study, we reduced the 3D model to 1D model prioritizing including electrophysiological details over including the 3D strain and stress fields since the previous study suggested that lateral stresses are negligibly small compared to longitudinal stress.[25] MCT Ca^{2+} gain is defined as the level of Ca^{2+} upregulation in response to stress applied to the cell. The functional form was defined according to the experimentally obtained Ca^{2+}-afterload relationship. We assumed that MCT-Ca^{2+} gain function affects $I_{Ca,L}$ and thus modulates electrophysiology. The cross-bridge force generation model by Negroni et al.,[29] which was tuned to reproduce Ca^{2+}, length, and velocity dependence of cross-bridge force development, was integrated into the Shannon-Bers model of rabbit ventricular cardiomyocyte.[28] The cross-bridge force is fed back to the mechanical equilibrium calculation to close the MCT feedback loop.

Our model is able to reproduce experimentally observed mechanical and electrophysiological responses, including prolonged APD, larger Ca^{2+} transient, and maintained shortening. MCT-Ca^{2+} gain dependence on changes in afterload also agreed with experimental results. Our model also makes nontrivial predictions that MCT enables autoregulation of contraction in the cardiomyocytes under a range of load changes but triggers electro-mechanical discordant alternans under excessively high loads.

RESULTS

Validation of the model on mechanical load effect on EC coupling

In Figure 2, we compared the simulated responses under load-free and in-gel contraction with experimental observations outlined by the green box. The black lines correspond to the

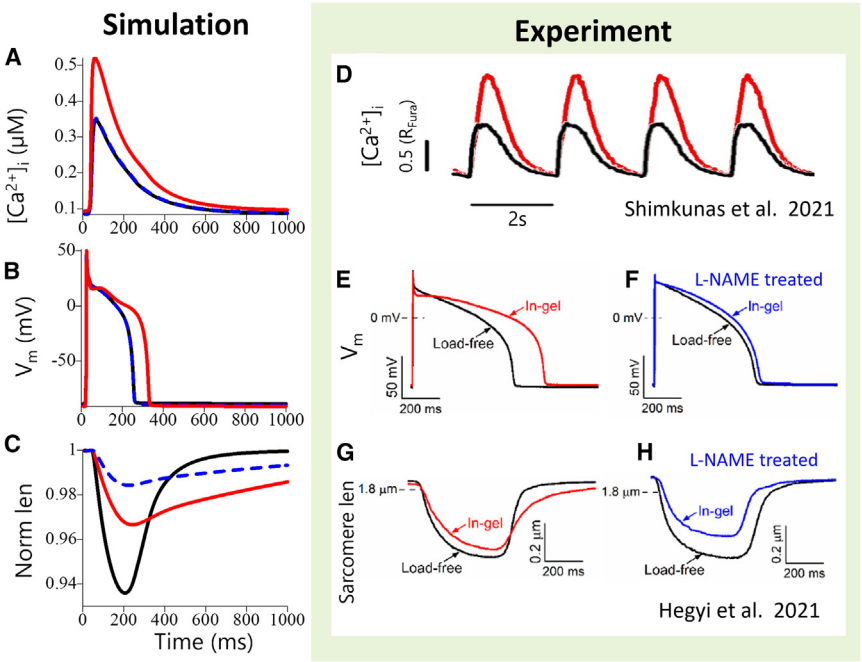

Figure 2. Validation of the new model on mechanical load effect on EC coupling

Time courses of simulated electrophysiological and mechanical responses under load-free (black), in-gel (red), and in-gel without MCT (blue) conditions (left panels) are compared with experimentally reported time courses (right panels in the green background). (D) is adapted with permission from Shimkunus et al. (2021)[20]; copyright 2021 Wolters Kluwer Health. (E and F) are reproduced from Hegyi et al. (2021)[24] under a CC BY-NC-ND license.

(Left panels) (A–C) The steady-state under 0.5Hz pacing is shown: (A) bulk cytosolic $[Ca^{2+}]$, (B) action potential, (C) normalized length of the cell. In B and C, in-gel without MCT (blue dashed) lines coincide with load-free (black) lines. (Right panels) Whole-cell patch-clamp experiments in isolated rabbit ventricular cardiomyocytes embedded in PVA gel and Tyrode's solution paced at 0.5 Hz.

(D) Increased Ca^{2+} transient was observed with the in-gel condition.

(E and F) Action potential was significantly prolonged under in-gel conditions (red) and was attenuated by nitric oxide synthase (which mediates mechano-chemo-transduction effect) inhibitor NG-nitro-L-arginine methyl ester (L-NAME) treatment (blue).

(G and H) Time course of sarcomere length in load-free (black), in-gel (red), and in-gel with L-NAME treatment (blue).

load-free condition, while the red line represents the in-gel condition with a 10% CL concentration. Load-free condition is achieved by giving 0% CL concentration in simulation, resulting in no connection to the boundary and no force from the gel. Under the in-gel condition, the maximum $[Ca^{2+}]_i$ increased by 53%, rising from 0.35 to 0.52 μM (Figure 2A), the plateau phase of the action potential was prolonged, resulting in a 31% longer APD (from 232 ms to 305 ms, measured at 90% repolarization) (Figure 2B), shortening amplitude got smaller, and length recovery was slower (Figure 2C). Figures 2D, 2E, and 2G (reprints from Hegyi et al.[20] and Shimkunas et al.[24]) show experimentally observed representative time courses of increased $[Ca^{2+}]_i$, prolonged APD, smaller shortening, and slower length recovery in the cell-in-gel system (with 10% CL concentration for Figure 2D and 7.5% CL concentration for Figures 2E–2H) compared to the load-free condition. The model behaviors closely match the observed changes in the cell-in-gel system.

Hegyi et al.[20] have shown that the observed changes in the responses are due to MCT feedback by comparing load-free, in-gel with and without NG-nitro-L-arginine methyl ester (L-NAME) treatment in the gel. L-NAME is an inhibitor of nitric oxide synthase, known to mediate mechano-chemo-transduction effects. In the experiment, L-NAME pretreatment nearly abolished the afterload-induced changes in APD and action potential profile (Figure 2F). Shortening in-gel with blunted MCT further decreased compared to the in-gel condition. The blue dashed lines in the simulation reproduced the in-gel experiment with L-NAME condition by removing MCT: giving the total-force value of zero to the MCT Ca^{2+} gain function regardless of the actual total force value obtained by solving mechanical equilibrium. As in the experiment, Ca^{2+} transient and action potential profiles coincide with those under load-free conditions, and fractional shortening (FS) was lessened than in-gel conditions. This means that decreased shortening by mechanical constraints was compensated by MCT-increased contractility to maintain the magnitude of shortening.

Autoregulation of EC coupling enabled by MCT feedback

We investigated the model's response to changes in afterload by changing CL concentration. In Figures 3A and 3B, time courses of $[Ca^{2+}]_i$ and normalized length at steady state during 0.5 Hz simulations for each CL concentration were presented. Afterload changed $[Ca^{2+}]_i$ amplitudes but had little effect on their profiles. On the other hand, CL concentration affected both shortening amplitude and profile. Increased CL concentration increases constraints in both directions, in forward as afterload and in backward as resistance for length recovery. Figure 3C shows time courses of $I_{Ca,L}$. The initial peak is less affected by afterload; MCT increases $I_{Ca,L}$ at the end phase of APD. This prolongs APD and increase the steady level of $[Ca^{2+}]_{SR}$ from 0.53 mM under LF to 0.58 mM under 10% CL concentration resulting in increased SR Ca^{2+} release.

The maximum $[Ca^{2+}]_i$ and FS were shown in Figure 3D and 3E for comparison with the experimental observation by Shimkunas et al.[24] in Figures 3F and 4G. Diagonally striped boxes represent in-gel without MCT condition. As shown in Figure 3D, without MCT feedback, the maximum $[Ca^{2+}]_i$ values remain unchanged regardless of CL concentration. In contrast, with MCT feedback, we observed that $[Ca^{2+}]_i$ increases as CL concentration increases until it reaches its peak at 10% CL, as in the experiment (3F). This larger $[Ca^{2+}]_i$ at higher CL concentrations significantly increased FS compared to in-gel-without MCT condition (3E).

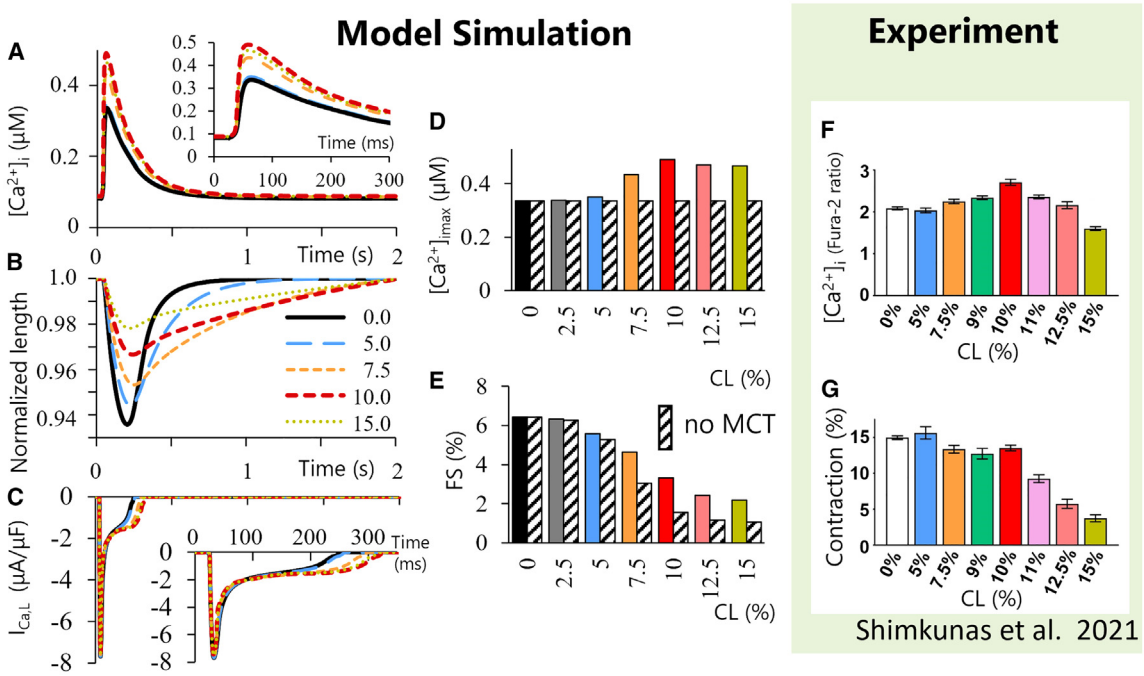

Figure 3. Autoregulation of EC coupling enabled by MCT feedback

The color indicates CL concentration, black: 0% (=load free), gray: 2.5%, blue: 5%, orange:7.5%, red: 10%, pink: 12.5%, and green: 15%.

(A) Time courses of simulated $[Ca^{2+}]_i$. The insets in (A) and (C) are enlarged views of the first 300 ms.

(B) Time courses of the simulated normalized length of the cell.

(C) Time courses of L-type Ca^{2+} channel current ($I_{Ca,L}$).

(D) Maximum intracellular $[Ca^{2+}]_i$ upon changing CL concentration. Diagonal striped boxes in (D) and (E) exhibit the results without MCT feedback.

(E) Fractional shortening on changing CL concentration.

(F) Experimental maximum intracellular $[Ca^{2+}]$ depending on CL concentration under 0.5Hz pacing.

(G) Experimental FS depending on CL concentration under 0.5Hz pacing. (F) and (G) on a green background are adapted with permission from Shimkunas et al.[24]; copyright 2021 Wolters Kluwer Health. Data are represented as mean ± SEM.

Increased FS mitigates a decline in shortening amplitude under high CL conditions. This maintenance of amplitude by MCT at high CL concentrations against larger loads qualitatively agrees with experimental observations (3G). These results show that our model reproduced the autoregulation of contractions, by increasing $[Ca^{2+}]_{SR}$ and $[Ca^{2+}]_i$ due to increased $I_{Ca,L}$ to compensate for higher mechanical constraints.

APD prolongation and alternans development under increasing mechanical load

Figure 4 upper panels in green (reprints from Hegyi et al.[20]) show representative time courses of action potentials and changes in APD_{90}, APD measured at 90% repolarization, under the increasing mechanical load condition by applying CL to PVA embedded cardiomyocyte under 0.5 Hz pacing. During the first 50 s in the load-free condition, APD_{90} was at the basal level of 600 ms. Just after the application of CL, APD started to prolong, as shown in 4C. The prolonged action potential profile is shown in comparison with the load-free profile in black (4A). Hegyi et al.[20] reported that some rabbit ventricular myocytes (19 out of 25 cells) progressively developed APD alternans after prolongation of APD (4C). Long action potentials are significantly longer (ΔAPD_{90}~300 ms) than short and load-free action potentials (4B). The duration between the application of the CL and the starting of alternans varied widely in the experiments.

We simulated the time course of APD_{90} with increasing afterload. While working with model parameters, we found that high CL concentration or increased amplitude of MCT-Ca^{2+} gain triggers alternans in our system.

In the experimental setup, CL is applied on the top surface of the PVA and CL spreads into the PVA by diffusion to form a gel of target viscosity. In order to simulate this experimental condition, we assumed that effective CL concentration can be expressed as $1 - \exp\left(\frac{\ln(0.1)t}{\tau_{gel0.1}}\right)$, reaching 90% of the target value within $\tau_{gel0.1} = 60$ s (Figure 4D). This assumption is based on the observation that experimentally, the gel stabilizes within a few minutes. The functional form is derived from the solution of the diffusion equation for a one-dimensional infinite plate problem, represented as the sum of an infinite series of $\exp(-\lambda_n t)$, where the first term is dominant.

Our model replicates APD prolongation upon the application of CL, followed by the emergence of alternans only when using amplified MCT-Ca^{2+} gain, $MCT_{1.5}$ (Figure 4E). Our model consistently replicates the phenomena independent of $\tau_{gel0.1}$, slower/faster increase in effective CL concentration. We note that the basal APD_{90} in our simulation was approximately 240 ms, which

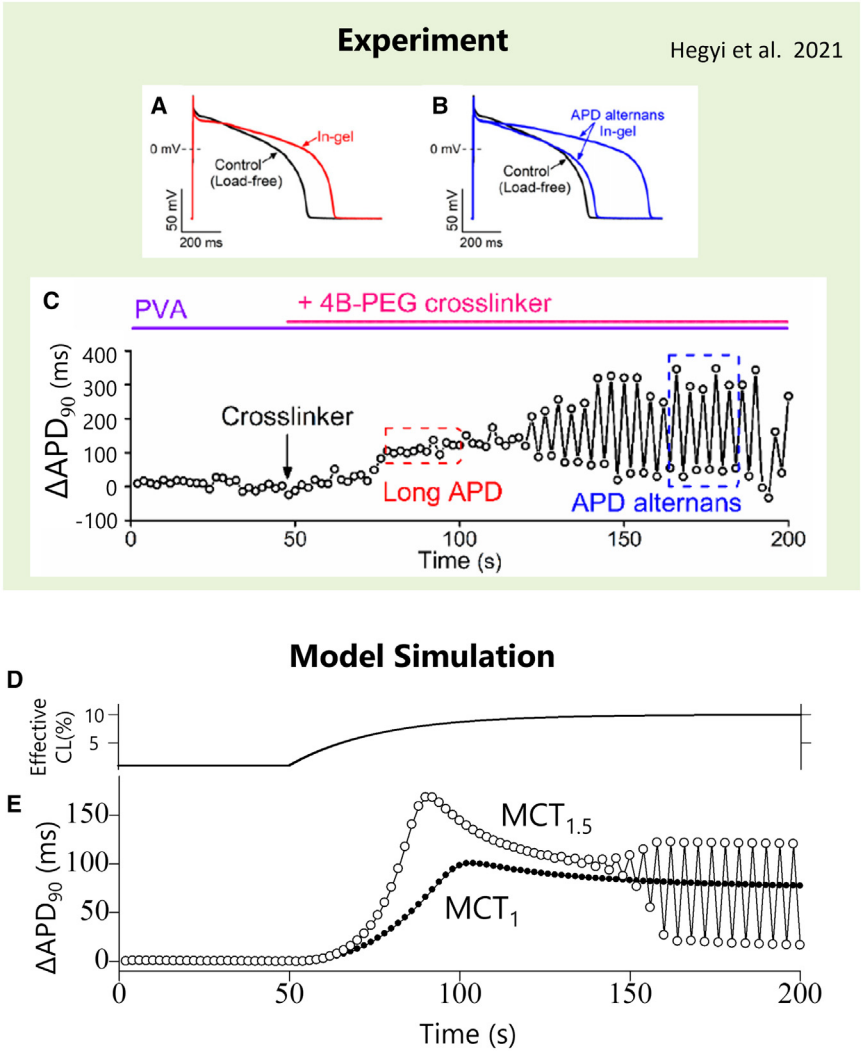

Figure 4. APD prolongation and alternans development under increasing mechanical load

(A–C) Representative time courses of action potential (A and B) and time development of ΔAPD_{90} (C) in the whole-cell patch-clamp experiments in isolated rabbit ventricular cardiomyocytes embedded in PVA under 0.5 Hz pacing at room temperature. The panels A, B, and C are reproduced from Hegyi et al. (2021)[20] under a CC BY-NC-ND license. After adding a cross-linker, a hydrogel formed around the cell to prolong APD (A, red) compared to load-free condition (black). Further gel stiffening often causes alternans, with longer APD significantly larger than that of load-free condition (B, blue).

(D) Suppositional effective cross-linker concentration for simulating responses on the application of the cross-linker. Exponential curve which reaches 9% CL (90% of the target concentration of 10% CL) after 60 s.

(E) Simulated ΔAPD_{90} in response to CL concentration change under MCT_1 (solid) and $MCT_{1.5}$ (open) are shown in D. APD_{90} prolongation occurred at first and subsequently, alternans were triggered under $MCT_{1.5}$. To replicate alternans development, 1.5 times amplified MCT-Ca^{2+} gain function $MCT_{1.5}$ was used (see Figure 5).

is shorter than that observed in the experiment (~600 ms). This difference is primarily due to temperature difference. Our model is designated for physiological temperature as in the Shannon-Bers model on which it is based, whereas the cell-in-gel experiment was conducted at room temperature.

Regarding transient behavior, APD exhibits three distinct phases. In both MCT_1 and $MCT_{1.5}$ cases, APD initially rises to a peak, then decreases, resulting in a hump-shaped time course. The third phase, however, differs between the two cases: with MCT_1 APD reaches a new stable value, while with $MCT_{1.5}$, it develops alternans. During the first phase, gel stiffness increases following the rise in CL concentration, leading to greater stress. The increased stress elevates $[Ca^{2+}]_i$ through MCT, and the higher $[Ca^{2+}]_i$ further amplifies stress, creating a positive feedback loop that enhances contraction. This loop halts when stress reaches the negative slope in the MCT-Ca^{2+} gain function, and the system shifts into the second phase. In this phase, $[Ca^{2+}]_i$ starts to decrease, while the rising CL continues to increase stress. In the third phase, CL reaches a plateau. With MCT_1, the system stabilizes at a new $[Ca^{2+}]_i$ value, whereas with $MCT_{1.5}$, which has a steeper negative slope, the system begins to oscillate. A hump during the initial increase in APD was not observed in experiments. This discrepancy with experimental observations suggests the need to incorporate additional variables into the MCT feedback loop or to introduce appropriate delays in MCT feedback. Although the transient behavior does not perfectly match experimental observations, our model successfully reproduces the increased $[Ca^{2+}]_i$ and APD under in-gel steady-state conditions as well as the triggered alternans with excessive feedback.

The effect of MCT-Ca^{2+} gain and functional form on EC coupling stability

To clarify which aspect of the MCT function contributed to the observed instability, we tested different MCT functions and amplitude. We started with $MCT_{1.5}$ which we observed to cause alternans as shown in Figure 4E (Figure 5A, orange triangles), and tested two other gain functions, MCT_{atan} and MCT_{gauss} (Figure 5A, blue circle dots and light blue x marks, respectively). MCT_{atan} is fitted to trace the rising curve of $MCT_{1.5}$ without a negative slope to test whether alternans would be triggered solely by stress-monotonically-increasing L-type calcium channel (LCC) upregulation. MCT_{gauss} is fitted to mimic the peak and downfall of $MCT_{1.5}$ without a value lower than 1 to evaluate whether LCC downregulation at excessive stress is crucial or the presence of negative slope is the key factor. Stability of the EC coupling dynamics was investigated by sweeping pacing cycle length (PCL) from 3000 to 300 ms while varying MCT-Ca^{2+}

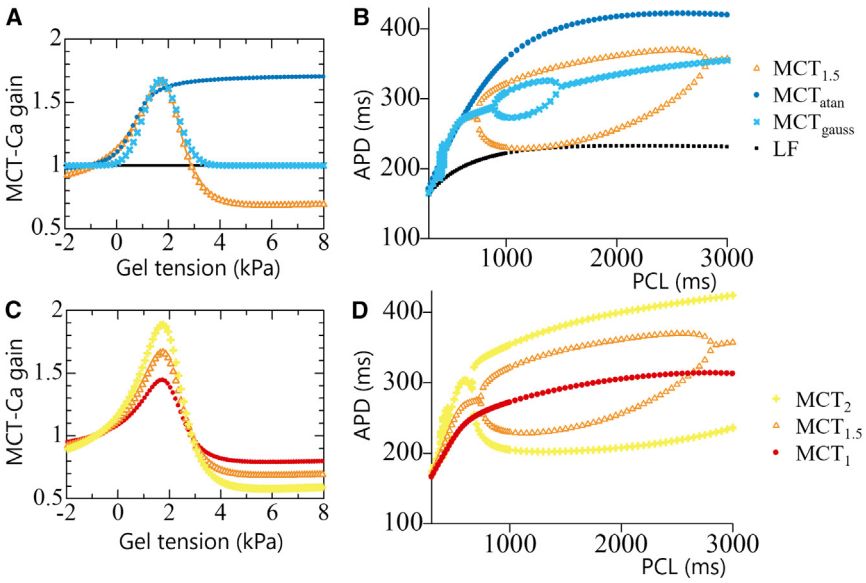

Figure 5. The effect of MCT-Ca^{2+} gain and functional form on EC coupling stability

(A) Three curves of the MCT function were tested. MCT_{gauss} (light blue x-mark) has the same peak as $MCT_{1.5}$ without downregulation of LCC ($MCT_{gauss} > 1$). MCT_{atan} traces the rising curve of $MCT_{1.5}$ and saturates without a negative slope (blue circle).

(B) Action potential duration (APD) in response to varying pacing cycle length (PCL) between 3000 and 300 ms with MCT functions in (A).

(C) The original MCT-Ca^{2+} gain function MCT_1 (red circle), amplified by 1.5 times (orange triangle) and 2.0 times (yellow plus).

(D) Action potentials with amplified MCT-Ca^{2+} gains shown in (C).

gain functional shape. In all the simulations, CL concentration was set to 10%. When using MCT_{atan}, we did not observe alternans (Figure 5B). Even when we amplified MCT_{atan}, we did not see alternans in a slower PCL range over 800 ms. When using MCT_{gauss}, alternans exists in a narrower PCL range between 1450 and 900 ms compared to $MCT_{1.5}$, between 2800 and 740 ms. This analysis suggests that the negative slope of MCT-Ca^{2+} gain is crucial for the development of alternans, but downregulation is not necessary.

Then, we also tested the effect of the amplitude of MCT-Ca^{2+} gain. The original MCT-Ca^{2+} gain MCT_1 was used to calculate Figures 2 and 3 results, and 1.5 and 2 times amplified $MCT_{1.5}$ and MCT_2 were examined (Figure 5C). Since MCT-Ca^{2+} gain is intended to multiply to the permeability of LCC, the value of one is the basal value; the differences from one were multiplied. The red circle indicates MCT_1, the orange triangle indicates $MCT_{1.5}$, and the yellow plus indicates MCT_2 in Figures 5C and 5D. MCT_1 muted alternans and MCT_2 widened the range of PCL with alternans compared to $MCT_{1.5}$; indicating that amplified MCT-Ca^{2+} gain destabilizes the system.

Mechanical load induced discordant alternans and mechanistic explanation

In Figure 6, we compared our simulated alternans with $MCT_{1.5}$ (6A) and experimentally observed alternans (6B) reprinted from Hegyi et al.[20] Both in the simulation and in the experiment, we observed higher [Ca^{2+}] in the sarcoplasmic reticulum ([Ca^{2+}]$_{SR}$) followed by larger Ca^{2+} release, larger cytosolic [Ca^{2+}], larger shortening amplitudes, and shorter APD. This means that the alternans were electromechanical discordant or AP/Ca discordant, which means that longer APD corresponds to smaller shortening and shorter APD corresponds to larger shortening. In our simulation, all alternans observed in slow pacing (PCL > ~800 ms) were electromechanical discordant. This observation aligns with the cell-in-gel experiment which also only observed electromechanical discordant alternans.

To investigate the mechanism, we also visualized stress, $I_{Ca,L}$, and the MCT-Ca^{2+} gain (Figure 6C). The MCT-Ca^{2+} gain is multiplied by $I_{Ca,L}$ at every timestep, providing instantaneous feedback to Ca^{2+} cycling based on mechanical conditions. For easier analysis, we named the beat with smaller shortening as the "red beat" and the subsequent beat as the "blue beat" and colored the graph accordingly. At the start of the red beat, the stored Ca^{2+} in SR is relatively low. This leads to a smaller Ca^{2+} transient and stress during the red beat. As the maximum level of stress is around the value where the MCT-Ca^{2+} gain function has its peak (~2 kPa), $I_{Ca,L}$ is well upregulated during contraction resulting in a longer APD. This larger Ca^{2+} influx and smaller release from SR in the red beat increased [Ca^{2+}]$_{SR}$ for the subsequent blue beat. The blue beat works oppositely. Higher [Ca^{2+}]$_{SR}$ leads to larger [Ca^{2+}]$_i$ and stress. The stress exceeds the range of MCT upregulation, causing lesser upregulation of $I_{Ca,L}$. This smaller $I_{Ca,L}$ results in a shorter APD, thus causing electromechanical discordant alternans.

DISCUSSION

Autoregulatory ECC model with MCT feedback

In this study, we developed a model of contraction autoregulation in cardiomyocytes by coupling mechanistic models of electrophysiology, Ca^{2+} signaling and mechanics, where MCT feedback plays an essential role in closing the autoregulatory loop. By determining the MCT-Ca^{2+} gain based on experimental data, our model successfully replicated electrical, chemical, and mechanical responses maintaining contraction amplitude under in-gel conditions. Furthermore, our model reproduced the autoregulation of contraction under a range of moderate loads, as well as discordant alternans under high loads observed in experimental data.

In our previous paper by Izu et al.,[21] we theoretically demonstrated that stress-sensor positive feedback on Ca^{2+} transient under cell-in-gel conditions can autoregulate contraction amplitude. Subsequently, in the paper by Kazemi-Lari et al.,[26] a mechanically faithful model reproduced this autoregulation of contraction. However, the model was phenomenological, where

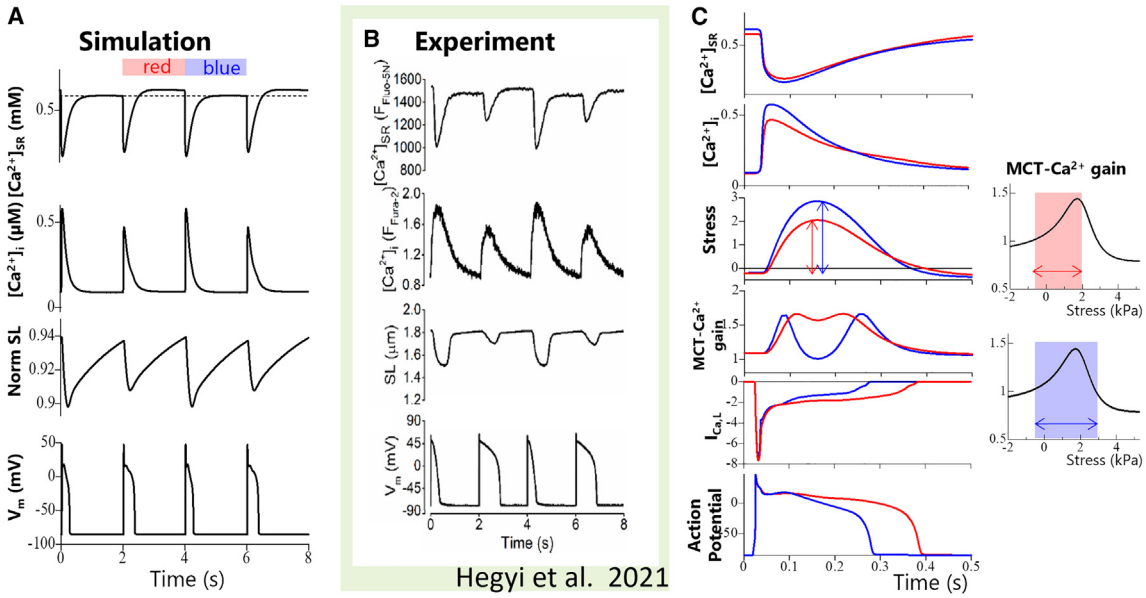

Figure 6. Mechanical load induced discordant alternans and mechanistic explanation

(A) Simulated intra-SR [Ca^{2+}], cytosolic [Ca^{2+}], normalized sarcomere length (SL), and action potential. The simulation was performed under 10% CL concentration with $MCT_{1.5}$ at 0.5Hz pacing.

(B) Experimentally reported alternans at 0.5 Hz pacing under cell-in-gel conditions. Figures are reproduced from Hegyi et al. (2021),[20] under a CC BY-NC-ND license.

(C) Comparison of time courses of two consecutive beats in alternans. Stress ranges in red and blue colored beats are indicated by red and blue arrows in the MCT-Ca^{2+} gain diagram. Lower intra-SR [Ca^{2+}] at the initiation of red-colored beat starting at 2 s leads to smaller Ca^{2+} transient and gel force exerted on the cell. Since this smaller force falls within the range of positive slope of MCT-Ca^{2+} gain, maintaining the gain high during the contraction. As a result, upregulated $I_{Ca,L}$ leads to longer APD. A larger Ca^{2+} influx and smaller release from SR lead to a higher SR load for the next beat colored in blue. The succeeding beat exhibits larger Ca^{2+} transient and gel force. Then gel force reaches the range of suppressive MCT-Ca^{2+} gain function, resulting in smaller $I_{Ca,L,}$ and shorter APD.

the Ca^{2+} transient was directly modulated by the stress without electrophysiological detail. The Ca^{2+} transient is modulated in a balance between SR and membrane Ca^{2+} handling which is strongly affected by electrophysiology. Building upon previous theoretical work by Izu et al. and the finite element model by Kazemi-Lari et al., our model here extends the understanding of autoregulation mechanisms by incorporating the MCT feedback into the excitation-contraction coupling (ECC) model, which allows for the evaluation of how electrical, chemical, and mechanical components interact within the system.

Our model can be considered as the first autoregulatory excitation-contraction coupling with MCT feedback model, unlike the traditional ECC models that typically operate as open-loop systems. In the traditional ECC models, electrophysiology determines Ca^{2+} transient, Ca^{2+} transient determines cross-bridge force, and cross-bridge force determines length and stress. While there are models that account for mechanics influencing cross-bridge force through the Frank-Starling mechanism, these models neglect the feedback effect of mechanics on electrophysiology. By incorporating MCT feedback, our model closes the feedback loop and enables modeling the stress-dependent autoregulation of the dynamic ECC coupling system.

MCT-Ca^{2+} gain and autoregulation of contraction

The theoretical analysis by Izu et al.[21] employed a closed-loop model with three variables: Ca^{2+} transient, cell contraction strain, and mechano-sensor strain. By assuming a lateral surface mechano-sensor model, they demonstrated that a positively monotonic and bounded feedback could replicate the biphasic response of Ca^{2+} transient and cell strain to the gel stiffness. In our model, the MCT-Ca^{2+} gain function corresponds to the feedback function from the mechano-sensor to the Ca^{2+} transient in Izu's theoretical model. While the functional form of MCT_{atan} follows the condition of being positively monotonic and bounded, only biphasic MCT functions can reproduce the biphasic Ca^{2+} transient response to gel stiffness. This difference arises from the assumptions made. We use total stress as the input for the feedback to electrophysiology, assuming a longitudinal mechano-sensor. The critical difference between the lateral-surface and longitudinal mechano-sensor is that the lateral-surface mechano-sensor strain approaches zero when gel stiffness becomes infinite, whereas the longitudinal mechano-sensor strain saturates to a maximum value. The model by Kazemi-Lari et al.[26] also adopted the longitudinal mechano-sensor assumption and employed a biphasic function to replicate the biphasic response of the Ca^{2+} transient.

In the current model, the adoption of a biphasic MCT-Ca^{2+} gain function enabled three key features: autoregulation of contraction under moderate afterload conditions, biphasic response of Ca^{2+} transient to the gel stiffness, and discordant alternans under high afterload conditions. While a monotonic function, like MCT_{atan} could replicate autoregulation and performed

better in maintaining contraction amplitude, it was not able to reproduce the biphasic response nor discordant alternans. As explained in Figure 6, the biphasic nature and alternans are strongly related. Since alternans can trigger arrhythmias, the suppression of Ca^{2+} under excessive afterload and the accompanying alternans might be a protective mechanism.

Validity of the simplified mechanical model

A previous simulation conducted by Kazemi-Lari et al.,[25] utilized the Eshelby inclusion theory to simulate the 3D nature of the stress-strain field. We compared our simplified mechanical model results with those by Kazemi-Lari et al.[25] to validate our simplification in the mechanical model (Figure S1). Under 10% CL concentration, our model yielded maximum and minimum gel stress values of 2.2 kPa and −0.32 kPa, respectively, with 56% of the negative tension persisting at the triggering of the next beat. Kazemi-Lari's model reported the maximum and minimum gel stress values of 1.85 kPa and −1.05 kPa, with 66% of the negative stress persisting. The time constant of gel stress attenuation during diastole, representing the reduction of the pushing force on the cell, was 183 ms, 428 ms, and 1122 ms in our simulation for 4%, 6%, and 8% CL, respectively. In a study by Kazemi-Lari et al.,[25] these values were 210 ms, 500 ms, and 1320 ms, respectively, in their Eshelby inclusion simulation.

The discrepancy in minimum gel stress can primarily be attributed to differences in systolic duration. Our simulation had a shorter systolic duration compared to the previous Eshelby inclusion simulation, which was based on experimental contractile force profiles.

Overall, the time courses of gel stress recovery and their dependency on CL concentration in our simplified 2-element mechanical model align well with the Eshelby inclusion simulation which considered the 3D nature of the system. However, in our simulation and Kazemi-Lari et al.'s simulation,[26] length returns slowly compared to the experimental observations. This difference is not solely due to the omission of the 3D nature of mechanics.

The nonlinearity of the gel's mechanical properties, which is ignored in both simulation studies, could be one of the causes of the discrepancy. The mechanical properties of the gel were obtained by a dynamical mechanical analyzer with a shear strain amplitude of 2%,[25] indicating that they are only valid in small strains. However, the maximum local strain expected in the finite element study was over 16%. Nonlinear elastic properties of the gel may contribute to the experimentally observed faster length recovery.[33,34]

The timescale of mechano-chemo-transduction

The destabilization of the system due to feedback time delays has been demonstrated through dynamical systems theory.[35] In cardiac electrophysiology model, the consideration of time delays due to Ca^{2+} transport in the SR was crucial for reproducing Ca^{2+}-driven alternans.[35] Discordant alternans observed in the cell-in-gel system provides an important clue to understanding the timescale of MCT and how arrhythmogenic activities may arise from the time delay and the magnitude of MCT-Ca^{2+} gain.

In our model, we used the current stress to calculate the mechanical feedback, which implies the feedback is instantaneously occurring beat-to-beat. The only delay component included in the current model is the delay caused by viscosity. We tested the case of pure-elastic gel (or surrounding material), without viscosity. On increasing elasticity, the system without viscous elements exhibited alternans at a certain elasticity when the force reached the negative slope of MCT. The instability triggered in the current model is not due to the viscous delay component.

In the cell-in-gel experiments, as shown in Figure 4, APD prolongation begins within a few beats after the addition of CL and stabilizes within a few minutes, which is in line with the expected rate of Ca^{2+} handling changes. This onset of APD prolongation indicates the involvement of rapid feedback mechanisms in the MCT system. For phenomena expected to exhibit instantaneous responses, mechanosensitive channels where mechanical stress or stretch directly influences the opening and closing of channel pores are conceivable. For example, the Piezo1 channel is proposed to function as a lever-like mechano-transducer, converting tension-induced conformational changes of the peripheral blade to the intracellular gate.[36,37] Similarly, TREK channels are reported to be regulated by tension of the cell membrane directly.[38,39]

Experimental data support the involvement of the NOS1-NO signaling and the CaMKII pathway as an essential part of the MCT pathway.[15,24,40,41] The NOS1-derived NO signal is known to be rapid occurring within milliseconds,[42,43] CaMKII-dependent Ca^{2+} channel facilitation occurs within seconds,[44,45] while the time courses of RyR activation are on the order of ∼3 min.[46] In addition to the NOS1-CaMKII pathway,[40] NADPH oxidase is reported to generate ROS and increase Ca^{2+} spark in response to stretch.[47] Mechanosensitive channels may also play a role in these phenomena. Since both the electrophysiology of cardiomyocytes and cell-in-gel mechanics are nonlinear dynamical systems, we cannot easily estimate the effects of those delay factors. To include those additional pathways, we may need separate MCT function for each pathway with respective amplitude, sensitivity to stress/strain, and delay. Further refinement of the model is on-going when more experimental data becomes available.

APD prolongation

The patch-clamp-in-gel experiments by Hegyi et al.[20] demonstrate that APD prolongation occurred in response to increased afterload on the cardiomyocyte contracting under mechanical load. This APD prolongation was abolished by inhibiting contraction to relieve the mechanical stress, confirming that the APD prolongation was caused by the mechanical load. Additional experimental evidence of mechanical load effects on APD lengthening comes from the *in vivo* electrocardiograph (ECG) measurement in the spontaneously hypertensive rat model, showing a positive correlation between the blood pressure and the QT interval which reflects APD.[48,49] The prolongation of QT interval has been observed in hypertension and is a risk predictor of cardiac arrhythmias.[48] In the whole animal, many factors may contribute to the QT interval prolongation, including increased ventricular mass, remodeling of ionic currents, and mechano-electric feedback. It is also known that BP is regulated by circadian rhythm,[50] and QT duration increases in conjunction with morning blood pressure peaks in hypertensive individuals.[51] However, the exact

cellular and molecular mechanisms remained unclear. The recent experimental study by Hegyi et al. and the present modeling study reveal a novel MCT mechanism that directly links APD prolongation to the mechanical stress in the ventricular myocytes contracting under afterload.

Remodeling of AP morphology under preload (mechanical strain by stretching the cell) was also studied in isolated cardiomyocytes.[9] The preload effect on AP is attributed to stretch-activated currents, which differ from the AP prolongation by afterload showing different reversal potential.[20] While mechanical stretch can either shorten or lengthen APD depending on the intensity and timing of the stretch,[9,18] cell-in-gel afterload consistently prolongs APD.[20] Our model successfully reproduced APD prolongation in the cell-in-gel mechanical environment by incorporating MCT feedback effects into the LCC current.

Mechanism underlying discordant alternans

In the cell-in-gel experiments, alternans is often observed and are all electro-mechanical discordant alternans, whereas rabbit cardiomyocytes under load-free conditions rarely exhibit discordant alternans. Electro-mechanical alternans, or AP/Ca discordant alternans, are characterized by long action potentials corresponding to small Ca transients and contractions.[22,23] A numerical study by Sato et al.[52] reported that Ca^{2+}-driven instability triggers discordant alternans while voltage-driven instability triggers concordant alternans. Discordance occurs under negative voltage-calcium coupling, where higher intracellular Ca^{2+} shortens action potential duration via calcium-dependent inactivation of $I_{Ca,L}$, rather than prolonging it via sodium-calcium exchanger current.[22] They further showed that under negative voltage-calcium coupling, increasing I_{SAC} promotes discordant alternans.[52]

Wang et al.[53] reported that NS5806, an activator of transient outward current I_{to}, triggers electro-mechanical discordant alternans, and the addition of an $I_{Ca,L}$ inhibitor changed alternans into electro-mechanical concordant. This finding is consistent with the observation of cell-in-gel discordant alternans exhibiting increased I_{to} and $I_{Ca,L}$. I_{to} modulates the time course and magnitude of the Ca^{2+} transient through its effects on $I_{Ca,L}$ current,[54] potentially causing the voltage-calcium coupling to shift negatively.

Suction electrode measurement of monophasic action potential (MAP) in the mechanically loaded heart showed that alternans was always associated with LVP alternans.[55] The phase of electrical alternans showed a constant discordant relation to peak ventricular pressure, indicating discordant alternans of AP and contraction.[56] Interestingly, optical mapping of AP and Ca in the mechanically unloaded heart showed concordant alternans of AP and Ca^{2+} transient.[57]

We were able to replicate the observed discordant alternans under longer PCL (over 1000 ms) in the electrophysiology model by introducing MCT feedback. Most models investigating proarrhythmic alternans focus on instability under shorter PCLs (~200 ms).[58,59] The Shannon-Bers model[28] has long been investigated in many studies to reveal rabbit cardiac electrophysiology[29,44,58,60,61]; however, none of them reported the replication of discordant alternans or calcium-driven alternans to our knowledge. In our model, alternans cannot be triggered without a negative slope in the MCT-Ca^{2+} gain function, even when the model's response to the changes in PCL was examined by varying the amplitude and the functional shape of MCT-Ca^{2+} gain. The negative slope of MCT-Ca^{2+} gain constitutes negative voltage-calcium coupling in our system, triggering discordant alternans. The results show that the MCT serves autoregulatory mechanism in response to afterload, whereas triggers instability in response to overload.

Multiscale investigations into MCT

Mechano-sensitive processes together with the electrical and Ca control systems form an integrated system for controlling the contraction of the cardiomyocyte.[2,62] This integrated system can autoregulate contraction in response to changes in the mechanical environment and can also lead to pathological remodeling.[11,13,63] The cell-in-gel experiment was developed to analyze the mechanism of contraction autoregulation in cardiomyocytes.[14,15,20,24] It should be noted that the mechanical environment in the cell-in-gel setup differs significantly from most studies of MEC, where mechanical strain is applied by stretching the cell membrane (i.e., uniaxial stretch, osmotic swelling, pipette suction, inflation, etc.). Different stress and strain fields on the cardiomyocyte may activate different mechanosensors. In the cell-in-gel setup, afterload-induced NOS1-NO signaling is thought to be mediated by costameres formed by the dystrophin-glycoprotein complex and the vinculin-talin-integrin system[20]; conversely, uniaxial stretching of the membrane in cardiomyocytes is mediated by microtubular deformation and NADPH-oxidase 2 activation.[64] The mechano-electric feedback model, integrating SAC currents and stretch-induced myofilament Ca^{2+} release into established electrophysiology models, targets membrane-stretching experiments.[65] Our model integrates stress-induced $I_{Ca,L}$ alterations, reproducing the cell-in-gel experiments. These experiments and modeling for each pathway will contribute to a more comprehensive understanding of the entire mechano-feedback system and its mechanisms in cardiomyocytes.

Reil et al. reported an isolated whole-heart experiment with controlled preload and afterload, showing that without preload, the heart can immediately elevate contractility,[41] which is consistent with the cell-in-gel experiment. However, interpreting results between whole-heart and isolated cardiomyocyte experiments is not straightforward. Recent hypotheses attribute the equilibrium between the two myosin head resting states to explaining the Frank-Starling mechanism[66] and the Anrep effect.[67] It is acknowledged that two myosin head states exist for un-attached-to-actin conditions: a quasi-helically ordered OFF state and an ON state where this helical ordering is lost, as unveiled by X-ray diffraction studies, or an energy-sparing super-relaxed (SRX) state and a high-energy-consuming disordered-relaxed (DRX) state demonstrated by myosin ATPase assays. While it has been considered that the SRX and DRX states are equivalent to the OFF and ON states, respectively, new evidence has shown that they have distinct properties and should be regarded as independent, though they correlate in some cases.[68] Even single molecules of cardiac myosin have been shown to exhibit load-dependent force generation.[69] Li et al.[70] demonstrated that inhomogeneity of resting sarcomere length

causes stretching and lengthening within a myofibril during a beat, suggesting that the assumption of homogeneous periodicity may not hold true. This inhomogeneity could further complicate our understanding of where mechanosensors are located within the cellular ultrastructure and which mechanical conditions they respond to. Our MCT model foundation would be a useful tool for integrating these experimental findings from microscopic to organ-level experiments.

Limitations of the study

First, we focused only on the mechanical load effects on modulating LCC, while numerous components of other electrical physiology systems are reported to be mechanosensitive.[9,20,71] While LCC is the most prominent, other mechanosensitive elements may also affect Ca^{2+} handling. For example, mechanosensitive K^+ channels and non-specific ion currents, I_{SAC} is reported to suppress voltage-driven concordant alternans and promote Ca^{2+}-driven discordant alternans.[52] CaMKII is also known to increase RyR Ca^{2+} sensitivity, opening probability, and leak,[72,73] upregulate SERCA through PLB phosphorylation,[72] and enhance magnitudes of $I_{Na,L}$ and I_{to}.[74,75] NADPH oxidase has been reported to generate ROS and induce Ca^{2+} sparks increase in response to mechanical stimuli.[47,64] NCX, LCC, and SERCA pump are all known to be sensitive to oxidation.[76] NO and CaMKII are also known to enhance NADPH oxidase,[77,78] and these two pathways interact.[40] Additionally, alterations in myofilament calcium sensitivity upon stretch observed as triggered propagating contractions[65,79,80] is another important mechanism affecting the coupled system. Incorporating these multiple pathways affecting multiple targets by defining respective MCT functions with appropriate sensitivity, amplitude, and time delays could represent the entire network, although many parameters remain unknown. Additionally, we will include or replace current models with those that are better-tuned for Ca^{2+}-handling,[59,81–84] alternans,[58] beta-adrenergic response,[29,85] or pathology,[86] depending on the purpose. While we acknowledge that attributing all MCT feedback only to LCC may be over-simplified, we consider the current model to be a good initial step for modeling closed-loop feedback of mechano-chemo-transduction in cardiac E-C coupling.

Second, for computational efficiency, we simulated the cell as a one-dimensional hyperelastic body and the gel as a viscoelastic environment. However, the mechanical stimuli are three-dimensional and may vary under different experimental conditions.[12,87] To incorporate a three-dimensional effect, we need to know the mechanosensor's effective deformation modes and their locations inside the cell. Different mechanosensors may have different effective deformation modes, such as uniaxial, bi-axial tension, and curvature for membrane proteins.[38,88] The local membrane deformation is expected to vary significantly depending on where it is in the cell architecture (ex. during shortening, the surface membrane may slack and the tubular membrane may stretch or curve[89]). Incorporating a more comprehensive 3D-MCT model would provide valuable insights when further information on mechanosensitive sensors is available.

In summary, despite the limitations mentioned previously, our closed-loop MCT model provides a valuable foundation for evaluating effects of MCT pathways in cardiomyocytes. With further improvements, this foundation could extend from evaluating the impact of experimental, molecular-level findings on cells to exploring and assessing pharmacological and therapeutic strategies targeting mechano-sensitive pathways. The conceptual innovation of the present model is to enable analyzing the autoregulation of E-C coupling dynamic system in the cardiomyocytes under mechanical load. The long-term goal is to understand how the heart autoregulates contractile force in response to load changes to maintain cardiac output, and why mechanical overload leads to arrhythmias and heart failure.

RESOURCE AVAILABILITY

Lead contact

Requests for further information and resources should be directed to and will be fulfilled by the lead contact, Asuka Hatano (hatano@fml.t.u-tokyo.ac.jp).

Materials availability

This study did not generate new unique reagents.

Data and code availability

- This paper analyzes published experimental data, accessible at https://doi.org/10.1073/pnas.2108484118, https://doi.org/10.1016/j.ijengsci.2021.103489, and https://doi.org/10.1161/CIRCRESAHA.120.318570.
- All original code has been deposited at https://github.com/UTokyo-FML/MCT2024.git and is publicly available at [https://doi.org/10.5281/zenodo.14269939].
- Any additional information required to reanalyze the data reported in this paper is available from the lead contact upon request.

ACKNOWLEDGMENTS

We gratefully acknowledge the colleagues and former trainees whose work provided the foundation for this paper, especially Dr. Jian Zhong, Dr. Bence Hegyi, Dr. Rafael Shimkunas, Dr. Marina Gabriel, Prof. Kit S. Lam, Dr. Mohammad A. Kazemi-Lari, and Prof. John Shaw (U, Michigan).

We also thank Prof. W. Jonathan Lederer, Prof. Donald M. Bers, Prof. Tamas Banyasz, Prof. Anthony Baker, and other colleagues who have contributed to scientific discussions over the years. We also thank Prof. Satoshi Izumi (U, Tokyo) and Prof. Yoichiro Mori (U, Pen) for scientific discussions.

Funding: This work was supported by the grants from United States National Institutes of Health (NIH). R01-HL149349 (to D.S.), R01HL149431 (to L.T.I.), R01HL090880 (to L.T.I. and Y.C.-I.), R01HL123526, R01HL141460, R01HL159993 to (Y.C.-I. and L.T.I.), and R35HL166575 Outstanding Investigator Award (to Y.C.-I.).

AUTHOR CONTRIBUTIONS

Conceptualization and investigation, A.H., D.S., Y.C.-I., and L.T.I.; methodology, A.H. and D.S.; software and validation, A.H.; resources, D.S., Y.C.-I., and L.T.I.; writing-original draft, A.H.; writing-review and editing, A.H., D.S., Y.C.-I., and L.T.I. All authors have read and approved the article.

DECLARATION OF INTERESTS

The authors declare no conflict of interest.

STAR★METHODS

Detailed methods are provided in the online version of this paper and include the following:

- KEY RESOURCES TABLE
- EXPERIMENTAL MODEL AND STUDY PARTICIPANT DETAILS

SUPPLEMENTAL INFORMATION

Supplemental information can be found online at https://doi.org/10.1016/j.isci.2025.111788.

Received: May 1, 2024
Revised: October 26, 2024
Accepted: January 8, 2025
Published: January 10, 2025

REFERENCES

1. Patterson, S.W., Piper, H., and Starling, E.H. (1914). The regulation of the heart beat. J. Physiol. *48*, 465–513. https://doi.org/10.1113/jphysiol.1914.sp001676.
2. Chen-Izu, Y., Shaw, J.A., Banyasz, T., and Izu, L.T. (2024). The Heart is a Smart Pump: Mechanochemotransduction Mechanism of the Frank-Starling Law and the Anrep Effect. Annu. Rev. Physiol. https://doi.org/10.1146/annurev-physiol-022724-104846.
3. von Anrep, G. (1912). On the part played by the suprarenals in the normal vascular reactions of the body. J. Physiol. *45*, 307–317. https://doi.org/10.1113/jphysiol.1912.sp001553.
4. Cingolani, H.E., Pérez, N.G., Cingolani, O.H., and Ennis, I.L. (2013). The Anrep effect: 100 years later. Am. J. Physiol. Heart Circ. Physiol. *304*, H175–H182. https://doi.org/10.1152/ajpheart.00508.2012.
5. Morris, C.E. (2011). Voltage-gated channel mechanosensitivity: fact or friction? Front. Physiol. *2*, 25. https://doi.org/10.3389/fphys.2011.00025.
6. Liang, J., Huang, B., Yuan, G., Chen, Y., Liang, F., Zeng, H., Zheng, S., Cao, L., Geng, D., and Zhou, S. (2017). Stretch-activated channel Piezo1 is up-regulated in failure heart and cardiomyocyte stimulated by AngII. Am. J. Transl. Res. *9*, 2945–2955.
7. Reed, A., Kohl, P., and Peyronnet, R. (2014). Molecular candidates for cardiac stretch-activated ion channels. Glob. Cardiol. Sci. Pract. *2014*, 9–25. https://doi.org/10.5339/gcsp.2014.19.
8. (2011). Cardiac Mechano-Electric Coupling and Arrhythmias (Oxford University Press). https://doi.org/10.1093/med/9780199570164.001.0001.
9. Peyronnet, R., Nerbonne, J.M., and Kohl, P. (2016). Cardiac Mechano-Gated Ion Channels and Arrhythmias. Circ. Res. *118*, 311–329. https://doi.org/10.1161/CIRCRESAHA.115.305043.
10. Kohl, P., Bollensdorff, C., and Garny, A. (2006). Effects of mechanosensitive ion channels on ventricular electrophysiology: experimental and theoretical models. Exp. Physiol. *91*, 307–321. https://doi.org/10.1113/expphysiol.2005.031062.
11. Quinn, T.A., and Kohl, P. (2021). Cardiac Mechano-Electric Coupling: Acute Effects of Mechanical Stimulation on Heart Rate and Rhythm. Physiol. Rev. *101*, 37–92. https://doi.org/10.1152/physrev.00036.2019.
12. Chen-Izu, Y., and Izu, L.T. (2017). Mechano-chemo-transduction in cardiac myocytes. J. Physiol. *595*, 3949–3958. https://doi.org/10.1113/JP273101.
13. Izu, L.T., Kohl, P., Boyden, P.A., Miura, M., Banyasz, T., Chiamvimonvat, N., Trayanova, N., Bers, D.M., and Chen-Izu, Y. (2020). Mechano-electric and mechano-chemo-transduction in cardiomyocytes. J. Physiol. *598*, 1285–1305. https://doi.org/10.1113/JP276494.
14. Shaw, J., Izu, L., and Chen-Izu, Y. (2013). Mechanical Analysis of Single Myocyte Contraction in a 3-D Elastic Matrix. PLoS One *8*, e75492. https://doi.org/10.1371/journal.pone.0075492.
15. Jian, Z., Han, H., Zhang, T., Puglisi, J., Izu, L.T., Shaw, J.A., Onofiok, E., Erickson, J.R., Chen, Y.J., Horvath, B., et al. (2014). Mechanochemotransduction during cardiomyocyte contraction is mediated by localized nitric oxide signaling. Sci. Signal. *7*, ra27. https://doi.org/10.1126/scisignal.2005046.
16. Peyronnet, R., Desai, A., Edelmann, J.-C., Cameron, B.A., Emig, R., Kohl, P., and Dean, D. (2022). Simultaneous assessment of radial and axial myocyte mechanics by combining atomic force microscopy and carbon fibre techniques. Philos. Trans. R. Soc. Lond. B Biol. Sci. *377*, 20210326. https://doi.org/10.1098/rstb.2021.0326.
17. Iribe, G., Ward, C.W., Camelliti, P., Bollensdorff, C., Mason, F., Burton, R.A.B., Garny, A., Morphew, M.K., Hoenger, A., Lederer, W.J., and Kohl, P. (2009). Axial stretch of rat single ventricular cardiomyocytes causes an acute and transient increase in Ca2+ spark rate. Circ. Res. *104*, 787–795. https://doi.org/10.1161/CIRCRESAHA.108.193334.
18. Nishimura, S., Seo, K., Nagasaki, M., Hosoya, Y., Yamashita, H., Fujita, H., Nagai, R., and Sugiura, S. (2008). Responses of single-ventricular myocytes to dynamic axial stretching. Prog. Biophys. Mol. Biol. *97*, 282–297. https://doi.org/10.1016/j.pbiomolbio.2008.02.011.
19. Yasuda, S.i., Sugiura, S., Yamashita, H., Nishimura, S., Saeki, Y., Momomura, S.i., Katoh, K., Nagai, R., and Sugi, H. (2003). Unloaded shortening increases peak of Ca2+ transients but accelerates their decay in rat single cardiac myocytes. Am. J. Physiol. Heart Circ. Physiol. *285*, H470–H475. https://doi.org/10.1152/ajpheart.00012.2003.
20. Hegyi, B., Shimkunas, R., Jian, Z., Izu, L.T., Bers, D.M., and Chen-Izu, Y. (2021). Mechanoelectric coupling and arrhythmogenesis in cardiomyocytes contracting under mechanical afterload in a 3D viscoelastic hydrogel. Proc. Natl. Acad. Sci. USA *118*, e2108484118. https://doi.org/10.1073/pnas.2108484118.
21. Izu, L., Shimkunas, R., Jian, Z., Hegyi, B., Kazemi-Lari, M., Baker, A., Shaw, J., Banyasz, T., and Chen-Izu, Y. (2021). Emergence of Mechano-Sensitive Contraction Autoregulation in Cardiomyocytes. Life *11*, 503.
22. Shiferaw, Y., Sato, D., and Karma, A. (2005). Coupled dynamics of voltage and calcium in paced cardiac cells. Phys. Rev. E Stat. Nonlin. Soft Matter Phys. *71*, 021903. https://doi.org/10.1103/PhysRevE.71.021903.
23. Sato, D., Shiferaw, Y., Garfinkel, A., Weiss, J.N., Qu, Z., and Karma, A. (2006). Spatially discordant alternans in cardiac tissue: role of calcium cycling. Circ. Res. *99*, 520–527. https://doi.org/10.1161/01.RES.0000240542.03986.e7.
24. Shimkunas, R., Hegyi, B., Jian, Z., Shaw, J.A., Kazemi-Lari, M.A., Mitra, D., Leach, J.K., Li, X., Jaradeh, M., Balardi, N., et al. (2021). Mechanical Load Regulates Excitation-Ca^{2+} Signaling-Contraction in Cardiomyocyte. Circ. Res. *128*, 772–774. https://doi.org/10.1161/CIRCRESAHA.120.318570.
25. Kazemi-Lari, M.A., Shaw, J.A., Wineman, A.S., Shimkunas, R., Jian, Z., Hegyi, B., Izu, L., and Chen-Izu, Y. (2021). A viscoelastic Eshelby inclusion model and analysis of the Cell-in-Gel system. Int. J. Eng. Sci. *165*, 103489. https://doi.org/10.1016/j.ijengsci.2021.103489.
26. Kazemi-Lari, M.A., Shimkunas, R., Jian, Z., Hegyi, B., Izu, L., Shaw, J.A., Wineman, A.S., and Chen-Izu, Y. (2022). Modeling cardiomyocyte mechanics and autoregulation of contractility by mechano-chemo-transduction feedback. iScience *25*, 104667. https://doi.org/10.1016/j.isci.2022.104667.
27. Bers, D.M. (2001). Excitation–Contraction Coupling and Cardiac Contractile Force (Springer). https://doi.org/10.1007/978-94-010-0658-3.
28. Shannon, T.R., Wang, F., Puglisi, J., Weber, C., and Bers, D.M. (2004). A mathematical treatment of integrated Ca dynamics within the ventricular myocyte. Biophys. J. *87*, 3351–3371. https://doi.org/10.1529/biophysj.104.047449.
29. Negroni, J.A., Morotti, S., Lascano, E.C., Gomes, A.V., Grandi, E., Puglisi, J.L., and Bers, D.M. (2015). beta-adrenergic effects on cardiac myofilaments and contraction in an integrated rabbit ventricular myocyte model. J. Mol. Cell. Cardiol. *81*, 162–175. https://doi.org/10.1016/j.yjmcc.2015.02.014.
30. Edwards, A.G., Grandi, E., Hake, J.E., Patel, S., Li, P., Miyamoto, S., Omens, J.H., Heller Brown, J., Bers, D.M., and McCulloch, A.D. (2014).

Nonequilibrium reactivation of Na+ current drives early afterdepolarizations in mouse ventricle. Circ. Arrhythm. Electrophysiol. *7*, 1205–1213. https://doi.org/10.1161/CIRCEP.113.001666.

31. Cortassa, S., Aon, M.A., O'Rourke, B., Jacques, R., Tseng, H.J., Marbán, E., and Winslow, R.L. (2006). A computational model integrating electrophysiology, contraction, and mitochondrial bioenergetics in the ventricular myocyte. Biophys. J. *91*, 1564–1589. https://doi.org/10.1529/biophysj.105.076174.
32. Toischer, K., Kögler, H., Tenderich, G., Grebe, C., Seidler, T., Van, P.N., Jung, K., Knöll, R., Körfer, R., and Hasenfuss, G. (2008). Elevated afterload, neuroendocrine stimulation, and human heart failure increase BNP levels and inhibit preload-dependent SERCA upregulation. Circ. Heart Fail. *1*, 265–271. https://doi.org/10.1161/CIRCHEARTFAILURE.108.785279.
33. Holzapfel, G.A. (1996). On Large Strain Viscoelasticity: Continuum Formulation and Finite Element Applications to Elastomeric Structures. Int. J. Numer. Methods Eng. *39*, 3903–3926. https://doi.org/10.1002/(sici)1097-0207(19961130)39:22<3903::aid-nme34>3.0.co;2-c.
34. Reese, S., and Govindjee, S. (1998). A theory of finite viscoelasticity and numerical aspects. Int. J. Solid Struct. *35*, 3455–3482. https://doi.org/10.1016/s0020-7683(97)00217-5.
35. MacDonald, N., and MacDonald, N. (2008). Biological Delay Systems: Linear Stability Theory (Cambridge University Press).
36. Wang, Y., Chi, S., Guo, H., Li, G., Wang, L., Zhao, Q., Rao, Y., Zu, L., He, W., and Xiao, B. (2018). A lever-like transduction pathway for long-distance chemical- and mechano-gating of the mechanosensitive Piezo1 channel. Nat. Commun. *9*, 1300. https://doi.org/10.1038/s41467-018-03570-9.
37. Geng, J., Liu, W., Zhou, H., Zhang, T., Wang, L., Zhang, M., Li, Y., Shen, B., Li, X., and Xiao, B. (2020). A Plug-and-Latch Mechanism for Gating the Mechanosensitive Piezo Channel. Neuron *106*, 438–451.e6. https://doi.org/10.1016/j.neuron.2020.02.010.
38. Maingret, F., Patel, A.J., Lesage, F., Lazdunski, M., and Honoré, E. (2000). Lysophospholipids Open the Two-pore Domain Mechano-gated K^+ Channels TREK-1 and TRAAK. J. Biol. Chem. *275*, 10128–10133. https://doi.org/10.1074/jbc.275.14.10128.
39. Enyedi, P., and Czirják, G. (2010). Molecular Background of Leak K+ Currents: Two-Pore Domain Potassium Channels. Physiol. Rev. *90*, 559–605. https://doi.org/10.1152/physrev.00029.2009.
40. Alim, C.C., Ko, C.Y., Mira Hernandez, J., Shen, E.Y., Baidar, S., Chen-Izu, Y., Bers, D.M., and Bossuyt, J. (2022). Nitrosylation of cardiac CaMKII at Cys290 mediates mechanical afterload-induced increases in Ca(2+) transient and Ca(2+) sparks. J. Physiol. *600*, 4865–4879. https://doi.org/10.1113/JP283427.
41. Reil, J.C., Reil, G.H., Kovács, Á., Sequeira, V., Waddingham, M.T., Lodi, M., Herwig, M., Ghaderi, S., Kreusser, M.M., Papp, Z., et al. (2020). CaMKII activity contributes to homeometric autoregulation of the heart: A novel mechanism for the Anrep effect. J. Physiol. *598*, 3129–3153. https://doi.org/10.1113/jp279607.
42. Fernando, V., Zheng, X., Walia, Y., Sharma, V., Letson, J., and Furuta, S. (2019). S-Nitrosylation: An Emerging Paradigm of Redox Signaling. Antioxidants *8*, 404.
43. Thomas, D.D., Liu, X., Kantrow, S.P., and Lancaster, J.R., Jr. (2001). The biological lifetime of nitric oxide: implications for the perivascular dynamics of NO and O2. Proc. Natl. Acad. Sci. USA *98*, 355–360. https://doi.org/10.1073/pnas.98.1.355.
44. Saucerman, J.J., and Bers, D.M. (2008). Calmodulin mediates differential sensitivity of CaMKII and calcineurin to local Ca2+ in cardiac myocytes. Biophys. J. *95*, 4597–4612. https://doi.org/10.1529/biophysj.108.128728.
45. Yuan, W., and Bers, D.M. (1994). Ca-dependent facilitation of cardiac Ca current is due to Ca-calmodulin-dependent protein kinase. Am. J. Physiol. *267*, H982–H993. https://doi.org/10.1152/ajpheart.1994.267.3.H982.
46. Huke, S., and Bers, D.M. (2007). Temporal dissociation of frequency-dependent acceleration of relaxation and protein phosphorylation by CaMKII. J. Mol. Cell. Cardiol. *42*, 590–599. https://doi.org/10.1016/j.yjmcc.2006.12.007.
47. Prosser, B.L., Ward, C.W., and Lederer, W.J. (2011). X-ROS Signaling: Rapid Mechano-Chemo Transduction in Heart. Science *333*, 1440–1445. https://doi.org/10.1126/science.1202768.
48. Klimas, J., Kruzliak, P., and Rabkin, S.W. (2015). Modulation of the QT interval duration in hypertension with antihypertensive treatment. Hypertens. Res. *38*, 447–454. https://doi.org/10.1038/hr.2015.30.
49. Klimas, J., Stankovicova, T., Kyselovic, J., and Bacharova, L. (2008). Prolonged QT Interval Is Associated with Blood Pressure Rather Than Left Ventricular Mass in Spontaneously Hypertensive Rats. Clin. Exp. Hypertens. *30*, 475–485. https://doi.org/10.1080/10641960802443399.
50. Okutucu, S., Karakulak, U.N., Sahiner, L., Aytemir, K., Demiri, E., Evranos, B., Fatihoglu, S.G., Kaya, E.B., Kabakci, G., Tokgozoglu, L., et al. (2012). The relationship between circadian blood pressure pattern and ventricular repolarization dynamics assessed by QT dynamicity. Blood Press. Monit. *17*, 14–19. https://doi.org/10.1097/MBP.0b013e3283502504.
51. Marfella, R., Gualdiero, P., Siniscalchi, M., Carusone, C., Verza, M., Marzano, S., Esposito, K., and Giugliano, D. (2003). Morning Blood Pressure Peak, QT Intervals, and Sympathetic Activity in Hypertensive Patients. Hypertension *41*, 237–243. https://doi.org/10.1161/01.HYP.0000050651.96345.0E.
52. Galice, S., Bers, D.M., and Sato, D. (2016). Stretch-Activated Current Can Promote or Suppress Cardiac Alternans Depending on Voltage-Calcium Interaction. Biophys. J. *110*, 2671–2677. https://doi.org/10.1016/j.bpj.2016.05.026.
53. Wang, S., Rodríguez-Mañero, M., Ibarra-Cortez, S.H., Kreidieh, B., Valderrábano, L., Hemam, M., Tavares, L., Blanco, E., and Valderrábano, M. (2019). NS5806 Induces Electromechanically Discordant Alternans and Arrhythmogenic Voltage-Calcium Dynamics in the Isolated Intact Rabbit Heart. Front. Physiol. *10*, 1509. https://doi.org/10.3389/fphys.2019.01509.
54. Sah, R., Ramirez, R.J., Oudit, G.Y., Gidrewicz, D., Trivieri, M.G., Zobel, C., and Backx, P.H. (2003). Regulation of cardiac excitation–contraction coupling by action potential repolarization: role of the transient outward potassium current (Ito). J. Physiol. *546*, 5–18. https://doi.org/10.1113/jphysiol.2002.026468.
55. Hirayama, Y., Saitoh, H., Atarashi, H., and Hayakawa, H. (1993). Electrical and mechanical alternans in canine myocardium *in vivo*. Dependence on intracellular calcium cycling. Circulation *88*, 2894–2902. https://doi.org/10.1161/01.CIR.88.6.2894.
56. Murphy, C.F., Lab, M.J., Horner, S.M., Dick, D.J., and Harrison, F.G. (1994). Regional electromechanical alternans in anesthetized pig hearts: modulation by mechanoelectric feedback. Am. J. Physiol. *267*, H1726–H1735. https://doi.org/10.1152/ajpheart.1994.267.5.H1726.
57. Choi, B.R., and Salama, G. (2000). Simultaneous maps of optical action potentials and calcium transients in guinea-pig hearts: mechanisms underlying concordant alternans. J. Physiol. *529*, 171–188. https://doi.org/10.1111/j.1469-7793.2000.00171.x.
58. Mahajan, A., Shiferaw, Y., Sato, D., Baher, A., Olcese, R., Xie, L.-H., Yang, M.-J., Chen, P.-S., Restrepo, J.G., Karma, A., et al. (2008). A Rabbit Ventricular Action Potential Model Replicating Cardiac Dynamics at Rapid Heart Rates. Biophys. J. *94*, 392–410. https://doi.org/10.1529/biophysj.106.98160.
59. Morotti, S., Grandi, E., Summa, A., Ginsburg, K.S., and Bers, D.M. (2012). Theoretical study of L-type Ca2+ current inactivation kinetics during action potential repolarization and early afterdepolarizations. J. Physiol. *590*, 4465–4481. https://doi.org/10.1113/jphysiol.2012.231886.
60. Soltis, A.R., and Saucerman, J.J. (2010). Synergy between CaMKII Substrates and β-Adrenergic Signaling in Regulation of Cardiac Myocyte Ca2+ Handling. Biophys. J. *99*, 2038–2047. https://doi.org/10.1016/j.bpj.2010.08.016.
61. Xie, Y., Grandi, E., Puglisi, J.L., Sato, D., and Bers, D.M. (2013). β-adrenergic stimulation activates early afterdepolarizations transiently via kinetic

mismatch of PKA targets. J. Mol. Cell. Cardiol. *58*, 153–161. https://doi.org/10.1016/j.yjmcc.2013.02.009.

62. Kohl, P., Hunter, P., and Noble, D. (1999). Stretch-induced changes in heart rate and rhythm: clinical observations, experiments and mathematical models. Prog. Biophys. Mol. Biol. *71*, 91–138.
63. Seo, K., Parikh, V.N., and Ashley, E.A. (2020). Stretch-induced biased signaling in angiotensin II type 1 and apelin receptors for the mediation of cardiac contractility and hypertrophy. Front. Physiol. *11*, 181.
64. Prosser, B.L., Ward, C.W., and Lederer, W.J. (2013). X-ROS signalling is enhanced and graded by cyclic cardiomyocyte stretch. Cardiovasc. Res. *98*, 307–314. https://doi.org/10.1093/cvr/cvt066.
65. Timmermann, V., Dejgaard, L.A., Haugaa, K.H., Edwards, A.G., Sundnes, J., McCulloch, A.D., and Wall, S.T. (2017). An integrative appraisal of mechano-electric feedback mechanisms in the heart. Prog. Biophys. Mol. Biol. *130*, 404–417. https://doi.org/10.1016/j.pbiomolbio.2017.08.008.
66. Lewalle, A., Milburn, G., Campbell, K.S., and Niederer, S.A. (2024). Cardiac length-dependent activation driven by force-dependent thick-filament dynamics. Biophys. J. *123*, 2996–3009. https://doi.org/10.1016/j.bpj.2024.05.025.
67. Sequeira, V., Maack, C., Reil, G.-H., and Reil, J.-C. (2024). Exploring the Connection Between Relaxed Myosin States and the Anrep Effect. Circ. Res. *134*, 117–134. https://doi.org/10.1161/CIRCRESAHA.123.323173.
68. Jani, V.P., Song, T., Gao, C., Gong, H., Sadayappan, S., Kass, D.A., Irving, T.C., and Ma, W. (2024). The structural OFF and ON states of myosin can be decoupled from the biochemical super-and disordered-relaxed states. PNAS nexus *3*, pgae039.
69. Liu, C., Kawana, M., Song, D., Ruppel, K.M., and Spudich, J.A. (2018). Controlling load-dependent kinetics of β-cardiac myosin at the single-molecule level. Nat. Struct. Mol. Biol. *25*, 505–514.
70. Li, J., Sundnes, J., Hou, Y., Laasmaa, M., Ruud, M., Unger, A., Kolstad, T.R., Frisk, M., Norseng, P.A., Yang, L., et al. (2023). Stretch harmonizes sarcomere strain across the cardiomyocyte. Circ. Res. *133*, 255–270.
71. Chen-Izu, Y., Jian, Z., Hegyi, B., Shimkunas, R., LariKazemi Lari, M.A., Shaw, J.A., Bers, D.M., Lam, K.S., and Izu, L.T. (2022). Autoregulation of excitation-Ca2+ signaling-contraction in cardiomyocyte under mechanical load. Biophys. J. *121*, 155a. https://doi.org/10.1016/j.bpj.2021.11.1952.
72. Soltis, A.R., and Saucerman, J.J. (2010). Synergy between CaMKII substrates and β-adrenergic signaling in regulation of cardiac myocyte Ca(2+) handling. Biophys. J. *99*, 2038–2047. https://doi.org/10.1016/j.bpj.2010.08.016.
73. Wehrens, X.H.T., Lehnart, S.E., Reiken, S.R., and Marks, A.R. (2004). Ca2+/calmodulin-dependent protein kinase II phosphorylation regulates the cardiac ryanodine receptor. Circ. Res. *94*, e61–e70. https://doi.org/10.1161/01.res.0000125626.33738.e2.
74. Wagner, S., Dybkova, N., Rasenack, E.C.L., Jacobshagen, C., Fabritz, L., Kirchhof, P., Maier, S.K.G., Zhang, T., Hasenfuss, G., Brown, J.H., et al. (2006). Ca 2+/calmodulin-dependent protein kinase II regulates cardiac Na+ channels. J. Clin. Invest. *116*, 3127–3138.
75. Wagner, S., Hacker, E., Grandi, E., Weber, S.L., Dybkova, N., Sossalla, S., Sowa, T., Fabritz, L., Kirchhof, P., Bers, D.M., and Maier, L.S. (2009). Ca/calmodulin kinase II differentially modulates potassium currents. Circ. Arrhythm. Electrophysiol. *2*, 285–294.
76. Zima, A.V., and Blatter, L.A. (2006). Redox regulation of cardiac calcium channels and transporters. Cardiovasc. Res. *71*, 310–321.
77. Girouard, H., Wang, G., Gallo, E.F., Anrather, J., Zhou, P., Pickel, V.M., and Iadecola, C. (2009). NMDA Receptor Activation Increases Free Radical Production through Nitric Oxide and NOX2. J. Neurosci. *29*, 2545–2552. https://doi.org/10.1523/jneurosci.0133-09.2009.
78. Lu, S., Liao, Z., Lu, X., Katschinski, D.M., Mercola, M., Chen, J., Heller Brown, J., Molkentin, J.D., Bossuyt, J., and Bers, D.M. (2020). Hyperglycemia Acutely Increases Cytosolic Reactive Oxygen Species via O-linked GlcNAcylation and CaMKII Activation in Mouse Ventricular Myocytes. Circ. Res. *126*, e80–e96. https://doi.org/10.1161/circresaha.119.316288.
79. Wakayama, Y., Miura, M., Sugai, Y., Kagaya, Y., Watanabe, J., Ter Keurs, H.E., and Shirato, K. (2001). Stretch and quick release of rat cardiac trabeculae accelerates Ca2+ waves and triggered propagated contractions. Am. J. Physiol. Heart Circ. Physiol. *281*, H2133–H2142.
80. Ter Keurs, H.E.D.J., Wakayama, Y., Miura, M., Shinozaki, T., Stuyvers, B.D., Boyden, P.A., and Landesberg, A. (2006). Arrhythmogenic Ca2+ release from cardiac myofilaments. Prog. Biophys. Mol. Biol. *90*, 151–171.
81. Stern, M.D., Ríos, E., and Maltsev, V.A. (2013). Life and death of a cardiac calcium spark. J. Gen. Physiol. *142*, 257–274. https://doi.org/10.1085/jgp.201311034.
82. Laver, D.R., Kong, C.H.T., Imtiaz, M.S., and Cannell, M.B. (2013). Termination of calcium-induced calcium release by induction decay: an emergent property of stochastic channel gating and molecular scale architecture. J. Mol. Cell. Cardiol. *54*, 98–100. https://doi.org/10.1016/j.yjmcc.2012.10.009.
83. Galice, S., Xie, Y., Yang, Y., Sato, D., and Bers, D.M. (2018). Size Matters: Ryanodine Receptor Cluster Size Affects Arrhythmogenic Sarcoplasmic Reticulum Calcium Release. J. Am. Heart Assoc. *7*, e008724. https://doi.org/10.1161/JAHA.118.008724.
84. Xie, Y., Yang, Y., Galice, S., Bers, D.M., and Sato, D. (2019). Size Matters: Ryanodine Receptor Cluster Size Heterogeneity Potentiates Calcium Waves. Biophys. J. *116*, 530–539. https://doi.org/10.1016/j.bpj.2018.12.017.
85. Bartos, D.C., Morotti, S., Ginsburg, K.S., Grandi, E., and Bers, D.M. (2017). Quantitative analysis of the Ca2+-dependent regulation of delayed rectifier K+ current IKs in rabbit ventricular myocytes. J. Physiol. *595*, 2253–2268.
86. Morotti, S., and Grandi, E. (2019). Quantitative systems models illuminate arrhythmia mechanisms in heart failure: Role of the Na(+) -Ca(2+) -Ca(2+)/calmodulin-dependent protein kinase II-reactive oxygen species feedback. Wiley Interdiscip. Rev. Syst. Biol. Med. *11*, e1434. https://doi.org/10.1002/wsbm.1434.
87. Sachs, F. (2010). Stretch-activated ion channels: what are they? Physiology *25*, 50–56. https://doi.org/10.1152/physiol.00042.2009.
88. Reeves, D., Ursell, T., Sens, P., Kondev, J., and Phillips, R. (2008). Membrane mechanics as a probe of ion-channel gating mechanisms. Phys. Rev. *78*, 041901. https://doi.org/10.1103/PhysRevE.78.041901.
89. Rog-Zielinska, E.A., Scardigli, M., Peyronnet, R., Zgierski-Johnston, C.M., Greiner, J., Madl, J., O'Toole, E.T., Morphew, M., Hoenger, A., Sacconi, L., and Kohl, P. (2021). Beat-by-Beat Cardiomyocyte T-Tubule Deformation Drives Tubular Content Exchange. Circ. Res. *128*, 203–215. https://doi.org/10.1161/CIRCRESAHA.120.317266.
90. Humphrey, J.D., Strumpf, R.K., and Yin, F.C. (1990). Determination of a constitutive relation for passive myocardium: II. Parameter estimation. J. Biomech. Eng. *112*, 340–346. https://doi.org/10.1115/1.2891194.
91. Humphrey, J.D., and Yin, F.C. (1987). On constitutive relations and finite deformations of passive cardiac tissue: I. A pseudostrain-energy function. J. Biomech. Eng. *109*, 298–304. https://doi.org/10.1115/1.3138684.
92. Linke, W.A., Popov, V.I., and Pollack, G.H. (1994). Passive and active tension in single cardiac myofibrils. Biophys. J. *67*, 782–792. https://doi.org/10.1016/S0006-3495(94)80538-7.
93. Hatano, A., Okada, J.i., Washio, T., Hisada, T., and Sugiura, S. (2011). A three-dimensional simulation model of cardiomyocyte integrating excitation-contraction coupling and metabolism. Biophys. J. *101*, 2601–2610. https://doi.org/10.1016/j.bpj.2011.10.020.
94. Flugge, W. (1967). Viscoelasticity (Blaisdell Publishing Company).
95. (2022). MATLAB Version: 9.13.0 (R2022b) (The MathWorks Inc).
96. Hatano, A. (2024). Mechano-Chemo-Transduction model of rabbit cardiomyocytes. Zenodo. https://doi.org/10.5281/zenodo.14269938.

STAR★METHODS

KEY RESOURCES TABLE

REAGENT or RESOURCE	SOURCE	IDENTIFIER
Software and algorithms		
Matlab R2024a	https://github.com/UTokyo-FML/MCT2024	https://doi.org/10.5281/zenodo.14269939

EXPERIMENTAL MODEL AND STUDY PARTICIPANT DETAILS

Mechanical equilibrium between cell and gel

Figure 1 upper left panel shows the mechanical model with one degree of freedom which corresponds to the cell-shortening and gel lengthening. This simplification allowed us to perform response analysis with varying force input in the time domain. The cell element consists of the cross-bridge force which is passed from the ECC model and the hyper-elastic model representing cell passive stress. The hyperelastic constitutive equations by Humphrey et al.[90,91] were restricted to the fiber direction to assure compatibility when extending the simulation to 3D in the future. Parameters fitted to a single myofibril experiment[92] were used from finite element simulation.[93] The cell is assumed to be 130 μm long surrounded by 100 μm long gel where experimentally detectable displacements were observed. Half of the system was modeled according to symmetric conditions. The gel element was modeled as the Generalized Maxwell model.[94] In the cell-in-gel experiment, afterload was manipulated by changing cross-linker (CL) concentration. We used the material parameters determined by Kazemi-Lari et al.,[21] expressed dependently on CL concentrations. This mechanical model with a hyperelastic cell and a generalized Maxwell gel replaced the one in the cross-bridge model by Negroni et al.[29] with a parallel passive element and a serial element attaching to the boundary. Nonetheless, the model retained the representation of sliding filaments with springs representing cross-bridge heads.

To solve the dynamic problem coupling with a viscoelastic element, which is dependent on the velocity, we took the time derivative of the hyperelastic equation to obtain velocity form. The generalized Maxwell model was written in incremental notation of viscoelastic forces and the common displacement velocity in all the parallel elements. Equilibrium was solved iteratively to obtain convergence of the nonlinear equation. The codes were all written in MATLAB.[95] Codes were verified by elongating the cell to simulate a hyper-elastic stress-strain relationship and by applying step strain input to the gel to simulate relaxation function. Codes were validated comparing with previous finite-element study[21] (Figure S1). The parameters are described in Tables S1 and S2.

MCT-Ca2+ gain

We chose cell total stress as an input to the MCT function as the cell total stress is the variable that reflects the afterload applied to the cell. There are three candidates for it in our model namely, cross-bridge force, cell-passive stress, and cell total stress (or gel stress, equal to the sum of cross-bridge force/area and cell-passive stress). The cross-bridge force is the input to mechanical equilibrium and cannot be an input to the MCT function since that connection skips the mechanical model. The previous study showed that the electrophysiological change under Cell-in-Gel is not by length or strain; in the presence of the myofilament contraction uncoupler blebbistatin, action potential with no-shortening did not differ from the load-free condition with large shortening.[20] Therefore, we did not choose the passive force for the MCT input since the passive force and the cell length are a one-to-one relationship.

We set LCC as the target of MCT feedback. The previous study showed that the $I_{Ca,L}$ was significantly increased under in-gel afterload condition (-6.3 A/F) compared to load-free condition (-4.8 A/F) during depolarizing pulses to +5 mV from holding potential of -40 mV.[20] The experimental relationship shows that $[Ca^{2+}]_{max}$ raises on increasing afterload, peaked at the afterload by 10% CL, and decreased to the level lower than load-free condition at 15% CL (Figure 3F). To reproduce these experimental observations, we set a functional form of MCT-Ca^{2+} gain by modifying the stress-Ca^{2+} MCT function in the model by Kazemi-Lari et al.[26] that could express the upregulation on increasing the stress in the moderate stress range and the downregulation in high stress (Figure 1 upper right) as follows:

$$MCT_1 = 1 + a_1 \frac{-d_0 F_{gel}\left(F_{gel} - d_1\right) + S_{min}}{d_2 + d_3\left(F_{gel} - d_1\right)^2}$$

, where $a_1 = 0.2, d_0 = 1.6, d_1 = 2, d_2 = 2, d_3 = 1.92$, and $S_{min} = 4$. To investigate the effects of the amplitude of the feedback, we tested $MCT_{1.5}$ and MCT_2, in which only a_1 value is multiplied by 1.5 and 2.0 respectively (Figure 5C). In addition, following two functional forms, MCT_{atan} and MCT_{gauss} are also used to examine the effects of the functional form.

$$MCT_{atan} = 1.32 + \frac{0.8 \operatorname{atan}\left(1.8\, F_{gel} - 1.2\right)}{\pi}$$

$$MCT_{gauss} = 1.0 + 1.1\frac{\exp\left(-0.5\left(F_{gel}-1.7\right)^2/\sigma^2\right)}{\sigma\sqrt{2\pi}}$$

, where $\sigma = 0.65$.

MCT_{atan} follows $MCT_{1.5}$ when stress is lower than the $MCT_{1.5}$ peak and then saturates without a negative slope. MCT_{gauss} is defined so that the peak and negative slope coincide with $MCT_{1.5}$ but without down-regulation (Figure 5A).

ECC model

The Shannon-Bers rabbit ventricular cardiomyocyte model[28] formulating electrical activities of ion channels and transporters, and Ca^{2+} transport mechanisms was combined with the cross-bridge force development model by Negroni et al.[29] The cross-bridge force development model well reproduces force-Ca^{2+}, force-length, and force-velocity relationships. A calculated cross-bridge force is used for the mechanical simulation. All the equations and parameters were the same as the original value in their paper except for the cell passive stiffness and multiplication of MCT-Ca^{2+} gain to the LCC current.

METHOD DETAILS

Closed loop of MCT

The proposed closed-loop model consists of three primary components (Figure 1): an excitation-contraction coupling (ECC) model, a mechanical model, and a mechano-transduction model. These components will be described in detail in the following sections. The interactions between these components are represented by the variables denoted in green boxes. The proposed MCT model calculates MCT-Ca^{2+} gain in response to the mechanical stress applied to the cell. This gain is used to modulate permeability of the L-type calcium channel (LCC), consequently up or down-regulating Ca^{2+} transient and contractility. For the sake of simplicity, this study focuses on the regulation of the LCC by MCT, ignoring other factors such as beta-adrenergic stimulation, or possible MCT effects on other channels. The ECC model simulates action potential, Ca^{2+} transient, and cross-bridge force. The calculated cross-bridge force is then transmitted to the mechanical model, where it influences the mechanical equilibrium between cell passive force and gel viscoelastic force. The mechanical model outputs stress, strain, length, and velocity of both the cell and the gel. The length and velocity of the cell directly affect the development of cross-bridge force in the ECC model. The stress applied to the cell by the gel, is fed back to the MCT model, thereby closing the feedback loop.

QUANTIFICATION AND STATISTICAL ANALYSIS

The whole program was coded in Matlab R2024a and is available in Github https://github.com/UTokyo-FML/MCT2024.git.[96] For the stability analysis, we used a dynamic pacing protocol. The pacing cycle length (PCL) was varied from 3000 to 1000 ms by 50 ms, and to 300 ms by 20 ms. At each PCL 300 beats were simulated using the final state of the previous PCL calculation as an initial condition. Each simulation of 300 beats took a few minutes on an Intel Core i7 2.8 GHz processor.